Acceleration-driven variable-density turbulent flow

Ilana Gat,[1] Georgios Matheou,[2] Daniel Chung,[3] and Paul E. Dimotakis[4]

[1]Graduate Aerospace Laboratories,
California Institute of Technology
igat@caltech.edu

[2]Jet Propulsion Laboratory,
California Institute of Technology
matheou@caltech.edu

[3]Mechanical Engineering,
University of Melbourne
daniel.chung@unimelb.edu.au

[4]Graduate Aerospace Laboratories,
California Institute of Technology
dimotakis@caltech.edu

Abstract

We discuss turbulent dynamics and mixing of a variable-density flow subject to a uniform-acceleration field. The flow resulting from initial misalignments of pressure and density gradients is investigated for small to large density ratios, with evidence that the small-density ratio flow is described by the Boussinesq approximation. A new shear-layer growth rate is reported. Spectra collapse when properly scaled for variable density.

1 Introduction

Turbulence and mixing between fluids of different densities responding to an externally imposed acceleration field, such as gravity, occur in many applications ranging from geophysics to astrophysics. The present study focuses on flow dynamics resulting from a body force, $\rho\,\mathbf{g}$, with ρ the local fluid density and $\mathbf{g} = -\widehat{\mathbf{z}}\,g$ the imposed uniform-acceleration field, in the zero Mach number limit.

Many flows can be treated as incompressible with small density variations, $\Delta\rho/\rho \ll 1$, and the Boussinesq approximation can often adequately describe the flow physics (e.g., Peltier and Caulfield, 2003, and references therein). Even though the Boussinesq linearization only accounts for the body force in the momentum equation (Batchelor et al., 1992) for small density variations, the Boussinesq linearization may capture the dynamics of misaligned hydrostatic pressure and density gradients in flows with small density variations. For the large density ratios studied, however, the Boussinesq linearization approximation cannot be used.

To study the effects of baroclinic torques, a flow configuration is considered in which two different gas-phase fluids are initialized with their density gradient perpendicular to the uniform-acceleration field. Density ratios in the range of $1.005 \leq R \equiv \rho_1/\rho_2 \leq 10$ are considered. In particular, it is presently found that even if this flow is initialized with near-unity density ratios, i.e., $R = 1+\epsilon$, which one would expect to tend to the Boussinesq approximation for small ϵ, its flow dynamics are statistically similar to large-density-ratio cases when properly scaled.

Generically, such flows are encountered in Rayleigh-Taylor instability, inertial-confinement fusion, as well as astrophysical and geophysical environments, such as in katabatic winds and Antarctic bottom-water (AABW) formation.

2 Problem formulation

The conservation of mass, momentum, and species-transport equations, absent species sources and sinks, are solved in the presence of the externally imposed uniform-acceleration field.

$$\frac{\partial \rho}{\partial t} + \nabla \cdot (\rho \mathbf{u}) \;=\; 0 \tag{1a}$$

$$\frac{\partial \rho \mathbf{u}}{\partial t} + \nabla \cdot (\rho \mathbf{u}\mathbf{u}) \;=\; -(\boldsymbol{\Gamma} + \nabla p) - \rho g \widehat{\mathbf{z}} + \nabla \cdot \boldsymbol{\tau} \tag{1b}$$

$$\frac{\partial \rho Y_\alpha}{\partial t} + \nabla \cdot [\rho Y_\alpha (\mathbf{u} + \mathbf{v}_\alpha)] \;=\; 0 \tag{1c}$$

where $\rho = \rho(\mathbf{x}, t)$ is the local binary-mixture density, $\mathbf{u}(\mathbf{x}, t)$ is the velocity vector, $p(\mathbf{x}, t)$ is the pressure, $\boldsymbol{\Gamma}$ is the uniform component of the pressure gradient, $Y_\alpha(\mathbf{x}, t)$ is the mass fraction of the α-species, and $\mathbf{v}_\alpha(\mathbf{x}, t)$ is the α-species diffusion velocity (e.g., Dimotakis, 2005). A Newtonian viscous stress tensor, $\boldsymbol{\tau}(\mathbf{x}, t)$, is assumed for monatomic gases (zero bulk viscosity).

The flow evolves with initial pure-fluid densities ρ_1, ρ_2, and $\rho_1 > \rho_2$. In the limit of zero Mach number, the only part in the species-diffusion velocity is that for Fickian transport, i.e., $\rho Y_\alpha \mathbf{v}_\alpha = -\rho \mathcal{D} \nabla Y_\alpha$, which with equations 1a and 1c yields the density-evolution equation,

$$\frac{\partial \rho}{\partial t} + \mathbf{u} \cdot \nabla \rho \;=\; -\rho \nabla \cdot \mathbf{u} \;=\; \rho \nabla \cdot \left(\frac{\mathcal{D}}{\rho} \nabla \rho \right) . \tag{1d}$$

Gas-phase molecular diffusion ($Sc = \nu/\mathcal{D} \approx 1$) is assumed, with a uniform dynamic viscosity, μ, leading to a variable diffusion coefficient, $\mathcal{D}(\mathbf{x}, t) = \mu/\rho(\mathbf{x}, t)$. Flow simulations set $\boldsymbol{\Gamma} = -\rho_0 g \widehat{\mathbf{z}}$, with $\rho_0 = \beta\rho_1 + (1-\beta)\rho_2$, where β is the volume fraction of high-density fluid in the domain. This choice ensures constant volume-averaged momentum.

This flow is studied by direct numerical simulation (DNS) in a triply-periodic cubic domain, initialized with high-density fluid between regions of low-density fluid, subject to an imposed uniform vertical acceleration field (Figure 1). A Fourier pseudo-spectral spatial-discretization method is used with a Helmholtz-Hodge decomposition of the pressure (Chung and Pullin, 2010) and a semi-implicit Runge-Kutta method (Spalart et al., 1991) for time integration.

3 Flow parameters

The flow domain is a triply periodic cube with a (dimensional) spatial extent scaled to $L = 4\pi$. The characteristic time, τ, and other parameters are scaled as,

$$\tau \;=\; 4\pi \sqrt{\frac{\ell}{\mathcal{A}\, g}} \tag{2}$$

$$\ell \;=\; \frac{L}{2} \tag{3}$$

$$\mathcal{A} \;=\; \frac{R-1}{R+1} \tag{4}$$

$$R \;=\; \frac{\rho_1}{\rho_2} \tag{5}$$

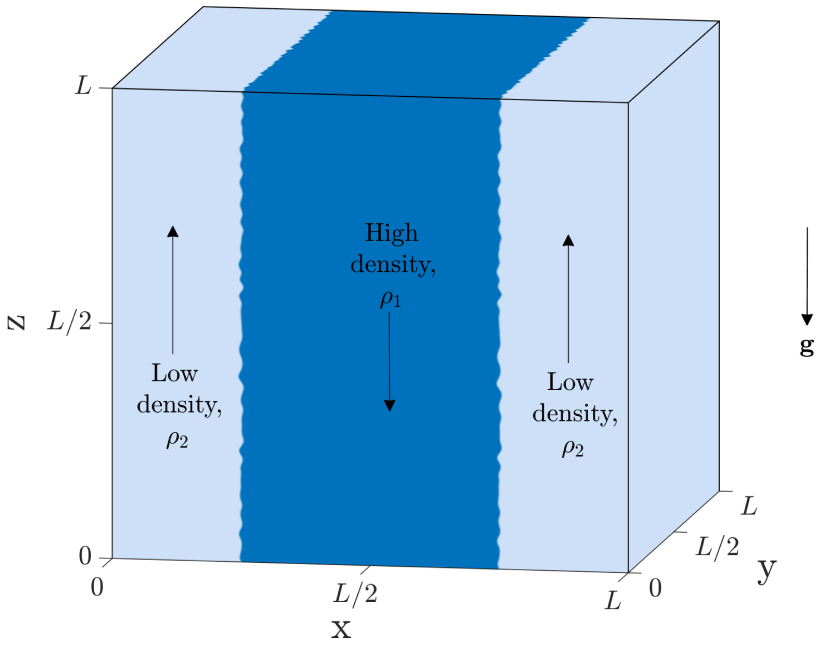

Figure 1: Simulation schematic of the perturbed initial density.

with $\mathcal{A}$ the Atwood number and $\mathcal{A}\,g$ the reduced acceleration. Additionally, $\rho_0 = 1$ always, which selects ρ_1 and ρ_2, given β and R. Figure 2 displays two-dimensional slices of the domain for flow with $R = 1.05$ at various non-dimensional times to illustrate its evolution. The flow initially is dominated by molecular diffusion, and then enters an unsteady regime characterized by eddy rollups. At later times, the flow becomes turbulent, and eventually homogenizes (because of domain periodicity).

4 Shear-layer growth

The mixed-fluid region (i.e., the shear layer), δ, is defined by a 1% criterion (Koochesfahani and Dimotakis, 1986), i.e., the extent within which the high-density fluid mass fraction, Y_1, is in the range

$$0.01 < Y_1 < 0.99 \tag{6}$$

where

$$Y_1(\mathbf{x},t) = \frac{\dfrac{1}{\rho(\mathbf{x},t)} - \dfrac{1}{\rho_2}}{\dfrac{1}{\rho_1} - \dfrac{1}{\rho_2}}\,. \tag{7}$$

Figure 3 displays the non-dimensional scaled shear-layer width over time for various density ratios. The flow is initialized with a finite transition width between the two fluids corresponding to an initial time, t_i. Scaling the initial shear-layer widths by this value collapses the data in the diffusive regime. In this regime, shear-layers grow as $\sqrt{t\,\mu/\rho_0}$, as expected, modulo an initial finite width, which is the natural scaling parameter of Equation 1a for $Sc = 1$. This is confirmed in the data in Figure 3. The flow subsequently transitions, monotonically with R, to a second regime of unsteady growth and eventually turbulence. Viscosity for the lower-R flow ($R < 1.05$) simulations was set higher than

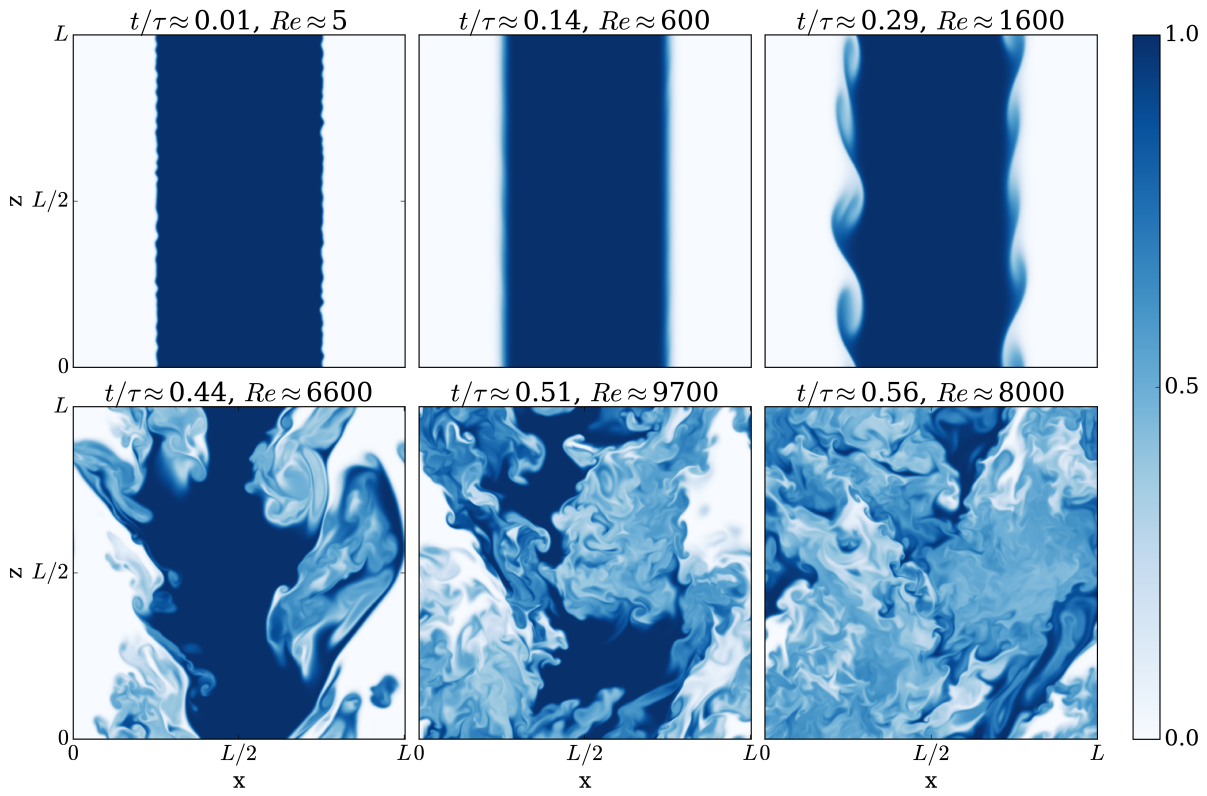

Figure 2: Two-dimensional slices of high-density fluid mole-fraction for $R = 1.05$. Reynolds numbers based on shear-layer width, δ.

it could have been, which may have affected their transition times from the diffusion-dominated regime. This second regime exhibits a cubic growth in time for the shear-layer width, i.e., $\delta(t) \sim (t + t_\mathrm{i})^3$. Slope changes at $\delta/\ell \approx 1$ mark encroachment of the turbulent region across the span of the free streams and the loss of pure free-stream fluid on either side of the shear layer at a location; the mixture begins to homogenize.

The unsteady/turbulent regime shear-layer width dependence on the cube of time is a robust result that holds for small to large density ratios. This can be explained by dimensional analysis and similarity arguments. The time rate of change of δ can be expressed in terms of scaled quantities, i.e.,

$$\frac{\mathrm{d}\,\delta}{\mathrm{d}(t/\tau)} \;\simeq\; \Lambda(t;\tau,R,g)\,. \tag{8a}$$

Λ has units of length, with a choice here similar to that for Rayleigh-Taylor (RT) flow,

$$\frac{\mathrm{d}\,\delta}{\mathrm{d}(t/\tau)} \;\propto\; \mathcal{A}\,g\,t^2\,. \tag{8b}$$

Non-dimensionalizing this equation yields the observed scaling (modulo virtual origins in t and δ),

$$\frac{\mathrm{d}\,(\delta/\ell)}{\mathrm{d}(t/\tau)} \;\simeq\; C_\delta \left(\frac{t}{\tau}\right)^2\,, \tag{8c}$$

where C_δ is a proportionality constant. We note that rescaling ℓ (or τ) would rescale C_δ, but would not alter the growth-rate power-law dependence on time.

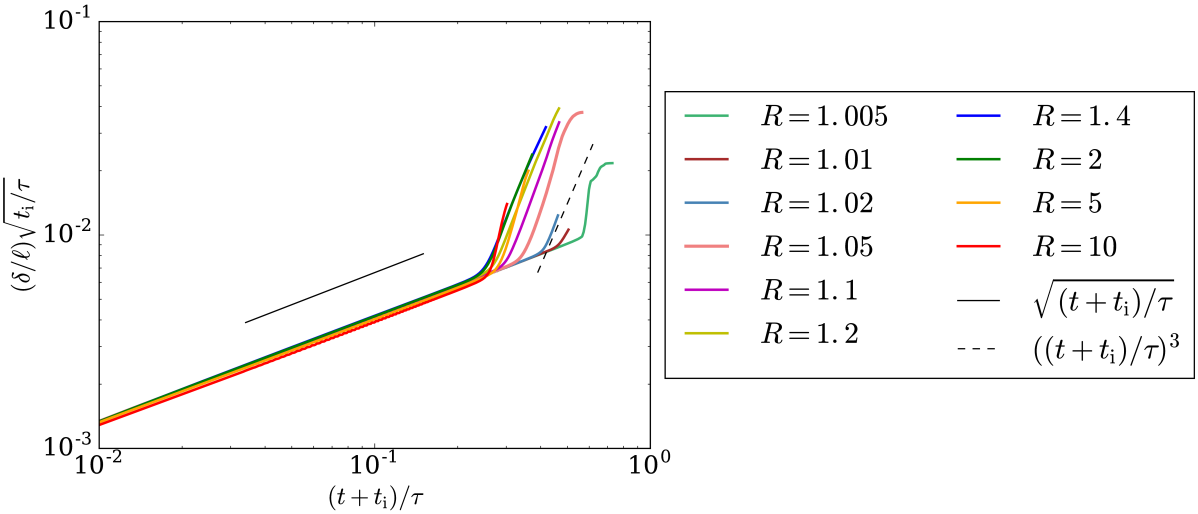

Figure 3: Non-dimensionalized shear-layer width, δ/ℓ, scaled by initial non-dimensional time. Colored lines are from simulations and black lines are slope references.

Other fast-growing flows, such as the vertical extent of the mixed-fluid region in RT flow, $h_{\mathrm{RT}}(t)$, also evolve in response to a uniform-acceleration field, e.g., gravity, and possess the same $\mathcal{A}\,g\,t^2$ length scale invoked in Equation 8b. However, the present flow has a characteristic time scale, τ, tied to a fixed length scale, ℓ, that has no RT counterpart. We note that δ in the present flow is a turbulent region *horizontal* width, whereas h_{RT} is the *vertical* extent of the RT turbulent region, governed by different dynamics.

Similar time scaling arises in buoyancy-dominated flows (Batchelor et al., 1992) and RT flows (Cook and Dimotakis, 2001). However, τ here corresponds to a pendulum-like flow period, inferred from Figure 2, and is that of a pendulum of length ℓ spanning the two free-stream mid-points in a reduced acceleration field, $\mathcal{A}\,g$. High-density fluid accelerates downwards with low-density fluid accelerating upwards, like an initially horizontal pendulum. This behavior is induced by the perpendicular (or misaligned) growth direction of the shear layer with the acceleration field direction, which does not govern the vertical extent growth in RT flow. However, the present flow is relevant to RT flow. The shear-layers here correspond to the regions between the "spikes" and "bubbles" in RT flow. The more rapidly growing shear-layers presented will encroach across the pure-fluid supply in RT flow, with a different very-late time growth regime expected that should be slower.

5 Spectra

Specific kinetic-energy spectra, $S_{\mathbf{u}\cdot\mathbf{u}}$, are compared to (full) kinetic-energy spectra in terms of $\mathbf{j} = \rho^{1/2}\mathbf{u}$ (Kida and Orszag, 1992). $S_{\mathbf{j}\cdot\mathbf{j}}/\overline{\rho}$ spectra are plotted (dashed lines) along with $S_{\mathbf{u}\cdot\mathbf{u}}$ spectra (specific-kinetic energy—solid lines), at a $Re \approx 8500$ attained for various density ratios, with the $R = 10$ case plotted at a slightly lower Re since it did not reach $Re \approx 8500$ (Figure 4). The two sets of spectra agree when scaled ($\overline{\rho}$ is the mean shear-layer density), for all R and Re investigated. Spectral agreement does not imply statistical independence; density and velocity are coupled in this flow. Variable-density kinetic-energy spectra can then be mapped to uniform-density spectra.

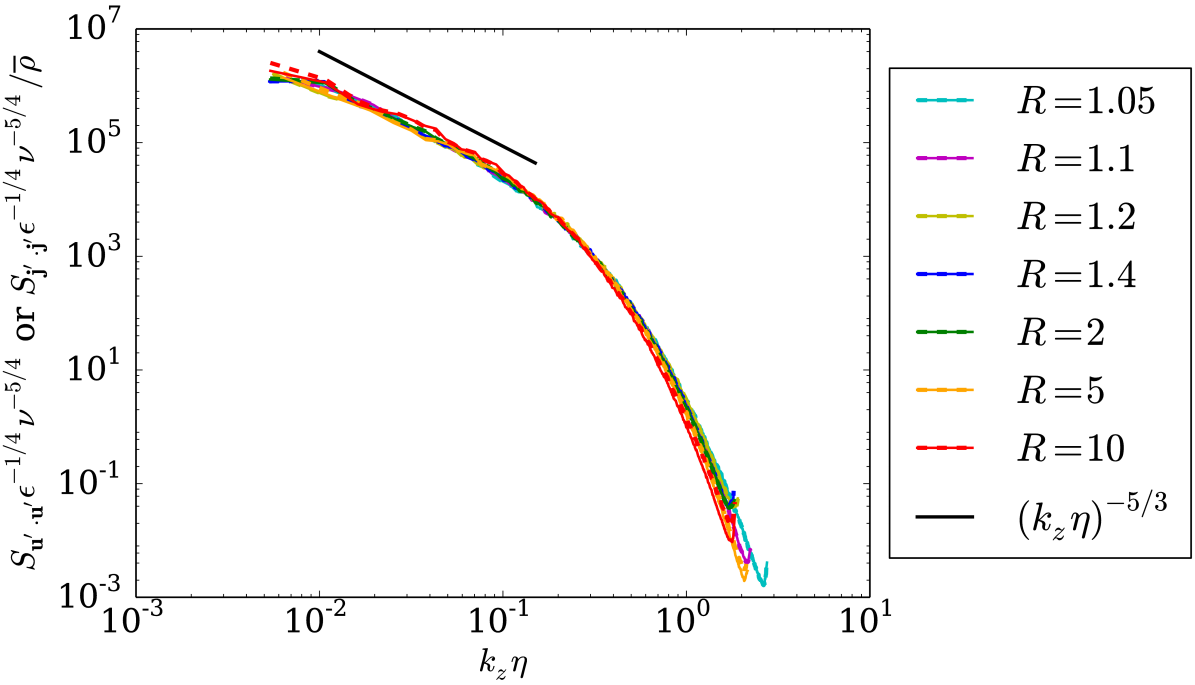

Figure 4: Specific kinetic energy spectra, $S_{\mathbf{u}\cdot\mathbf{u}}$ (solid), and kinetic energy spectra, $S_{\mathbf{j}\cdot\mathbf{j}}/\overline{\rho}$ (dashed), at $Re \approx 8500$, where $\mathbf{j}\cdot\mathbf{j} = \rho\mathbf{u}\cdot\mathbf{u} = \rho u^2$.

6 Conclusions

The behavior of variable-density turbulence in the flow studied can be mapped to uniform-density turbulence in term of spectral scaling. A new finding is the shear-layer width growth is cubic in time in the unsteady/turbulent regime, $\delta(t) \sim (t + t_\mathrm{i})^3$, which is consistent with a fixed imposed time scale, τ.

Acknowledgements

The work is supported by DOE Grant DE-NA0002382, AFOSR Grant FA9550-12-1-0461, NSF GRFP under Grant DGE-1144469, Caltech, and Blue Waters PRAC, supported by NSF OCI-0725070 and ACI-1238993, and Illinois. Data-storage/-visualization computer cluster, integrated by Daniel Lang and developed with support by NSF MRI Grant EIA-0079871, is used. Computations are also performed on the Caltech Zwicky computer cluster, supported by NSF MRI-R2 PHY-0960291 and by the Sherman Fairchild Foundation. The work was also supported by the Cray Trinity system of ACES, a partnership between LANL and SNL for the U.S. DOE's NNSA. We would like to acknowledge discussions with Profs. Dan Meiron and Dale Pullin, and the collaboration with Prof. Christian Ott in the computations.

References

Batchelor, G. K., Canuto, V. M., and Chasnov, J. R. (1992). Homogeneous buoyancy-generated turbulence. *J. Fluid Mech.*, 235:349–378.

Chung, D. and Pullin, D. I. (2010). Direct numerical simulation and large-eddy simulation of stationary buoyancy-driven turbulence. *J. Fluid Mech.*, 643:279–308.

Cook, A. W. and Dimotakis, P. E. (2001). Transition stages of Rayleigh–Taylor instability between miscible fluids. *J. Fluid Mech.*, 443:69–99.

Dimotakis, P. E. (2005). Turbulent mixing. *Annu. Rev. Fluid Mech.*, 37(1):329–356.

Kida, S. and Orszag, S. A. (1992). Energy and spectral dynamics in decaying compressible turbulence. *J. Sci. Comput.*, 7(1):1–34.

Koochesfahani, M. M. and Dimotakis, P. E. (1986). Mixing and chemical reactions in a turbulent liquid mixing layer. *J. Fluid Mech.*, 170:83–112.

Peltier, W. R. and Caulfield, C. P. (2003). Mixing efficiency in stratified shear flows. *Annu. Rev. Fluid Mech.*, 35:135–167.

Spalart, P. R., Moser, R. D., and Rogers, M. M. (1991). Spectral methods for the Navier–Stokes equations with one infinite and two periodic directions. *J. Comput. Phys.*, 96(2):297 – 324.

Note: An error was noted in the alignment statistics of vorticity and baroclinic torques in the originally posted paper and conference presentation. The present typescript is an update without the corresponding sections. The authors regret the original error.